

# EXPLOITING A NUMERICAL METHOD TO TRANSLATE SINGLE TOOTH BENDING FATIGUE RESULTS INTO MESHING GEARS DESIGN DATA: THE INFLUENCE OF MATERIAL PROPERTIES

F. CONCLI, L. MACCIONI & L. FRACCAROLI

Faculty of Science and Technology, Free University of Bolzano, Italy.

## ABSTRACT

According to standards, a fundamental gear design parameter, which heavily influences the sizing of these mechanical components, is the gear tooth root bending strength. To establish this parameter in a reliable way, tests should be performed on running gears (RG) manufactured with the same material and heat treatments under investigation. However, it is common practice in industry and in academia to perform single tooth bending fatigue (STBF) tests, which, on the one hand, are simpler and cheaper to perform, on the other hand, the stress history ( $\bar{\sigma}(t)$ ) they induce is not identical to that obtained during RG meshing. Therefore, it is necessary to apply a correction coefficient ( $f_{korr}$ ) to translate data obtained via STBF in RG design data. In recent studies, a method to estimate  $f_{korr}$ , through the combination of finite element (FE) simulations and the implementation of multiaxial fatigue criteria (MFC) based on the critical plane concept has been proposed. This method consists of simulating through FE a gear geometry both in the RG load case and in the equivalent STBF condition. Through the load histories recorded on the nodes belonging to the critical area, it is possible, by implementing different MFC, to identify the most critical node and the relative Damage Parameter (DP). The ratio between the obtained critical DP of the STBF case and RG provides the value of  $f_{korr}$ . However, different MFC can lead to different results in terms of  $f_{korr}$ . This is because different MFC differs in the definition of the DP. More specifically, DPs are both functions of material properties, such as the fatigue limit of the material related to symmetric sinusoidal bending stresses ( $\sigma_f$ ) and the fatigue limit at sinusoidal cyclic torsional stresses ( $\tau_f$ ), and load-dependent characteristics. The goal of this paper is to investigate the effect of different material properties, i.e.  $\sigma_f$  and  $\tau_f$ , on the estimation of  $f_{korr}$  highlighting differences between the various MFC implemented, i.e. Findley, Matake, Papadopoulos, and Susmel *et al.* To this respect, the above-mentioned numerical method has been applied to a specific gear geometry whose material properties have been systematically varied. Results show that the criteria of Findley and Papadopoulos lead to very similar results and a monotonically increasing relationship between  $f_{korr}$  and  $\tau_f/\sigma_f$ . A similar trend is observed for the Susmel *et al.* criterion but with higher value of  $f_{korr}$ . Differently, the criterion of Matake leads to a monotonic decreasing relationship between  $f_{korr}$  and  $\tau_f/\sigma_f$ .

*Keywords:* Critical plane, FEM, gears, material characterization, multiaxial fatigue, STBF.

## 1 INTRODUCTION

Gears are undoubtedly the most common solution to transfer mechanical power between different shafts, and their failure could lead to extraordinary maintenance operations and/or to damages with disastrous consequences [1]. To this respect, gears are potentially affected to several failure modes [2]. For example, an elevated pressure due to the meshing contact and/or an inadequate lubrication could lead to failure phenomena such as pitting [3], wear [4], scuffing [5], and micro pitting [6]. In addition, the fatigue load of the meshing teeth boosts the nucleation and the propagation of defects in the tooth radius region that, in turn, lead to complete tooth breakage [7–10]. This latter failure mode is called tooth root bending fatigue

(TBF); as it can be easily inferred, it is the most dangerous failure mode that could occur in a gear transmission [7–10]. For this reason, TBF strength has to be achieved as a priority in gear design [10].

To this respect, ISO 6336-3 [11] and ANSI/AGMA 2001 [12] are the two main standards in which a method to overcome TBF is proposed. According to the above-mentioned standards, for establishing the load carrying capacity of a gear, it is possible to compare the effective stress acting on the tooth root  $\sigma_F$  and the permissible one  $\sigma_{FP}$ . Moreover, ISO 6336-3 method B [11] states that  $\sigma_{FP}$  is directly proportional to admissible material strength  $\sigma_{Flim}$ . For new materials, the latter parameter is usually established through experimental tests, i.e. running gears (RG) tests [10, 13] or single tooth bending fatigue (STBF) tests [14–17].

Through RG tests, the effective state of stress – stress history ( $\bar{\sigma}(t)$ ) – that is acting on the gear teeth can be reproduced [10, 18]. This permits the exact estimation of  $\sigma_{Flim}$  [19]. In RG tests, the specimen is a gear manufactured with the material, heat treatments, and machining procedure to be investigated [10, 18]. It engages with one or more other gears that provide a specific torque under an appropriate lubrication condition. The end of the tests consists of the failure of the specimens (i.e. propagation of a crack in the tooth root region) and the overcoming of the run-out condition [10]. Acquiring additional failure values requires the use of another specimen. This, together with the need to have a test rig dedicated to these types of tests, makes RG tests very expensive and complex [15].

To simplify testing and reduce costs for obtaining representative fatigue values of  $\sigma_{Flim}$ , it is possible to perform STBF tests. As for RG tests, also in STBF tests, the specimen consists of a gear manufactured with the material to be tested having the specific characteristics to be investigated, i.e. heat treatment, machining procedure, etc. However, in STBF tests, multiple measurements can be performed on the same gear, and a common fatigue machine equipped with specific (but cost-effective) equipment can be exploited [20, 21]. Indeed, during STBF tests, the specimen is not rotating but only two teeth are loaded through two anvils without any lubrication. Therefore, the tooth breakage allows the same specimen to be used for further measurements.

In STBF tests, two anvils with parallel faces load the two teeth flanks that satisfy the Wildhaber property [1]. In this way, a pulsating force can be applied to the above-mentioned teeth, and the forces result in perfectly normalized flanks for the teeth and tangent to the base circle of the specimen [17]. However, the  $\bar{\sigma}(t)$  that STBF tests induce on the tooth root region is slightly different to those induced through RG tests, and, therefore, the evaluation of  $\sigma_{Flim}$  through STBF tests is inaccurate. In particular, STBF tests tend to overestimate the value of  $\sigma_{Flim}$  [22, 23]. As mentioned above, this fact can be explained by analyzing the differences between the stress histories of these two types of tests that are not considered by ISO 6336.

Discrepancies of  $\bar{\sigma}(t)$  can be explained as follows: First, during pulsatory tests, in order to keep the specimen in the right position, a constant load is applied. A typical ratio between the maximum load applied and the load needed to maintain the specimen in the correct position is defined at  $R = 0.1$ , e.g. STBF tests conducted in refs. [18, 24–28]. Naturally, this is not needed in normal meshing tests where  $R = 0$ , thus the effective stress acting on the teeth changes [13, 15, 29, 30]. Second, in STBF tests, the load is always applied in the same direction; it does not change during the experiment. This fact is not true for the classic RG test, in which the force vector varies in both magnitude and direction. In addition, in RG tests, an uneven share of loads is also present due to the simultaneous engagement of multiple

teeth [31]. This means that the stress time history at the tooth root is not sinusoidal as in the STBF tests [13, 15].

To consider the above-mentioned difference, it is possible to introduce a corrective factor ( $f_{korr}$ ) to translate STBF results into the RG ones [32]. The coefficient  $f_{korr}$  is the ratio between the  $\sigma_{Flim}$  obtained with the STBF approach and the  $\sigma_{Flim}$  calculated through RG tests. It has to be noticed that it is possible to use this correction factor only if the two tests are reproducing the same  $\sigma_F$ . In the literature, a very limited number of works in which this correction factor was predicted through experiments are present, e.g. Rettig [22] and Stahl [23]. Most of the recent literature refers to the use of numerical methods to estimate  $f_{korr}$ . In particular, numerical methods involving finite element analysis (FEA) of gears combined with multiaxial fatigue criteria (MFC) are usually employed.

For instance, in refs. [31, 33, 34], the scholars present innovative approaches that rely on the combination of FEA of gears and the Crossland fatigue criterion [35]. In ref. [36], the FEA results of a gear have been analyzed with the Liu & Mahadevan fatigue criterion [37]. In refs. [20, 21], the FEA results of different gears have been processed with the Findley's criterion [38] to estimate  $f_{korr}$ . With the same goal as in ref. [39], the FEA of a gear has been combined with the criteria of Findley [38], Matake [40], McDiarmid [41], Papadopoulos [42], and Susmel et al. [43]. In ref. [44], experimental results obtained with STBF tests have been compared with the numerical results achieved with the combination of FEA and various fatigue criteria based on the critical plane concept [45]. STBF numerical results have also been investigated in ref. [46] where different critical plane criteria have been applied to FEA of gears.

However, the characterization of a new material ( $\sigma_{Flim}$ ) by numerical estimation of  $f_{korr}$  combined with STBF experimental testing requires additional experimental tests for proper application [45]. Indeed, to be properly implemented, all MFCs necessitate the knowledge of at least two fundamental characteristics of the studied material, i.e. the fatigue limit of the material related to symmetric sinusoidal bending stresses ( $\sigma_f$ ) and the fatigue limit at sinusoidal cyclic torsional stresses ( $\tau_f$ ). Therefore, the purpose of this paper is to understand how variations in  $\tau_f$  and  $\sigma_f$  values could affect  $f_{korr}$  for different MFC.

In this respect, in Section 2, the numerical method to elaborate  $\bar{\bar{\sigma}}(t)$  through different MFC (starting from the knowledge of  $\tau_f$  and  $\sigma_f$ ) is presented. In Section 3, the FEAs carried out, the framework exploited to translate  $\bar{\bar{\sigma}}(t)$  on each nodes to  $f_{korr}$ , and the strategy adopted for the systematic variation of  $\tau_f$  and  $\sigma_f$ , are presented. In Section 4, results are presented and discussed. In Section 5, conclusions are provided.

## 2 BACKGROUND

In this paper, MFC that relies on critical plane concept are exploited. Therefore, in this paragraph, a brief introduction of the most important MFC based on the critical plane concept (i.e. Findley [38], Matake [40], Papadopoulos [42], and Susmel et al. [43]) is presented. Considering the stress tensor  $\bar{\bar{\sigma}}(t)$  (stress history) for a determined point in a specific time interval  $T$  (Equation 1), it is possible to use eqn 2 for computing the maximum octahedral stress  $\sigma_{h,max}$ . Considering eqn 3,  $\bar{\bar{I}}$  is the identity matrix and  $\sigma_\theta$  is the vector that, at a certain time  $t$ , contains the principal stresses that satisfy the relation reported in eqn 3.

Moreover, considering a plane that is described by a generic normal vector  $\mathbf{n}(\phi_n, \theta_n)$ , it is possible, using eqn 4, to compute the stress vector  $\mathbf{P}_n$  that is acting on that plane. The stress vector  $\mathbf{P}_n$  is time-dependent, which means that both its direction and modulus may change during a defined time interval (Fig. 1a). This vector can be divided into two components; a

normal component  $\sigma_n$  (eqn 5) and a tangential component  $\tau_n$  (eqn 6). The normal component  $\sigma_n$  has a fixed direction and the module is variable during time, while the tangential component  $\tau_n$  is completely time-dependent in terms of modulus and direction. In addition, the tangential component can also be divided into two directions, namely,  $u$  and  $v$  (eqn 6) (Fig. 1b). Where  $n, u, v$  are defined in eqn 7.

$$\bar{\bar{\sigma}}(t) = \begin{bmatrix} \sigma_{xx}(t) & \tau_{xy}(t) & \tau_{xz}(t) \\ \tau_{yx}(t) & \sigma_{yy}(t) & \tau_{yz}(t) \\ \tau_{zx}(t) & \tau_{zy}(t) & \sigma_{zz}(t) \end{bmatrix} \quad (1)$$

$$\sigma_{h,max} = \max_T \left\{ \frac{1}{3} \sum_{i=1,2,3} \sigma_{O_i} \right\} \quad (2)$$

$$\det |\bar{\bar{\sigma}}(t) - \sigma_O \bar{I}| = 0 \quad (3)$$

$$\mathbf{P}_n(\phi_n, \theta_n, t) = \bar{\bar{\sigma}}(t) \mathbf{n}(\phi_n, \theta_n) \quad (4)$$

$$\sigma_n(\phi_n, \theta_n, t) = \mathbf{n}^T(\phi_n, \theta_n) \bar{\bar{\sigma}}(t) \mathbf{n}(\phi_n, \theta_n) \quad (5)$$

$$\tau_n(\phi_n, \theta_n, t) = \mathbf{u}^T(\phi_n, \theta_n) \bar{\bar{\sigma}}(t) \mathbf{u}(\phi_n, \theta_n) + \mathbf{v}^T(\phi_n, \theta_n) \bar{\bar{\sigma}}(t) \mathbf{v}(\phi_n, \theta_n) \quad (6)$$

$$\mathbf{n}(\phi_n, \theta_n) = \begin{bmatrix} \cos \phi_n \sin \theta_n \\ \sin \phi_n \sin \theta_n \\ \cos \theta_n \end{bmatrix}; \mathbf{u}(\phi_n, \theta_n) = \begin{bmatrix} -\sin \theta_n \\ \cos \phi_n \\ 0 \end{bmatrix}; \mathbf{v}(\phi_n, \theta_n) = \begin{bmatrix} -\cos \phi_n \cos \theta_n \\ -\sin \phi_n \cos \theta_n \\ \sin \theta_n \end{bmatrix}; \quad (7)$$

In the case of stresses that are cyclic or, in other words, periodic, the stress vector  $\mathbf{P}_n$ , if watched in three dimensions, creates a curve that closes on itself and, by projection,  $\tau_n$  describes a closed loop in the plane. This curve is called  $\Gamma_n$  (Fig. 1b). The normal component of the stress vector  $\sigma_n$ , during a certain time period  $T$ , assumes different values from a minimum  $\sigma_{n,min}$  to a maximum  $\sigma_{n,max}$  (Fig. 1b). Thus, thanks to eqn 8, it is possible to evaluate the cyclic stress that is acting on the plane  $\sigma_{n,a}$  that has a normal vector  $\mathbf{n}$ .

$$\sigma_{n,a} = \max_T \{ \sigma_n(t) \} - \min_T \{ \sigma_n(t) \} = \sigma_{n,max} - \sigma_{n,min} \quad (8)$$

Considering the plane defined by the normal vector  $\mathbf{n}$  and the load history (stress cycle), it is possible to find, through the curve  $\Gamma_n$ , the components of tangential stresses. In the literature, there are several works in which different approaches for translating the curve  $\Gamma_n$  into a cyclic value of tangential stress  $\tau_{n,a}$  are presented. The most commonly used method is the minimum circumscribed circle (MCC) (eqn 9) [47]; with this approach, the alternate tangential stress  $\tau_{n,a}$  is calculated as the radius of the smallest circle that comprehends the whole curve  $\Gamma_n$  (Fig. 2).

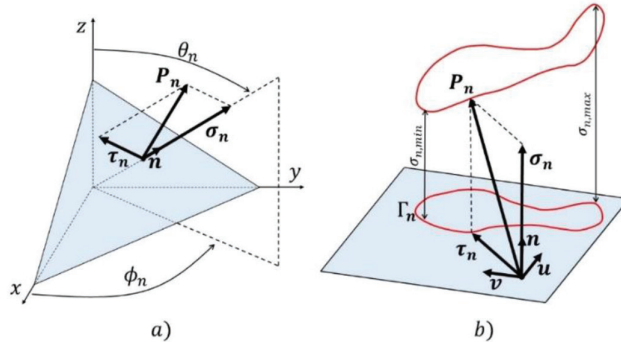


Figure 1: (a) Components of  $P_n(\phi_n, \theta_n, t)$  on the plane  $n(\phi_n, \theta_n)$  and (b) definition of the curve  $\Gamma_n$ .

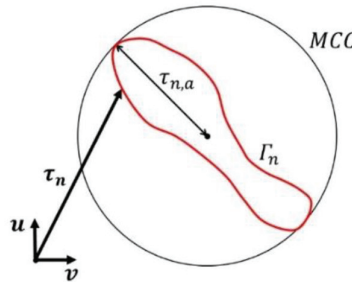


Figure 2: Minimum circumscribed circle (MCC) method.

$$\tau_{n,a} = MCC_T \{ \tau_n(t) \} \quad (9)$$

As before mentioned, considering a plane that has a normal vector  $\mathbf{n}$  that can be defined by  $\phi_n$  and  $\theta_n$ , it is possible to compute the stress parameters  $\tau_{n,a}$ ,  $\sigma_{n,max}$ , and  $\sigma_{n,a}$ . Moreover, it is possible to transform these parameters into spherical coordinates. In this work, these parameters are presented with the subscript  $c(\phi_c, \theta_c, \tau_{c,a}, \sigma_{c,max}, \text{and } \sigma_{c,a})$  when the plane  $\mathbf{n}$  coincides with the critical plane. The methods used to define when this happens are explained below.

Considering each MFC, based on the critical plane, it is possible to compute the damage parameter (DP) by using eqn 10. In which,  $S$  is the variable that represents the normal component of stress that is acting on the critical plane, and  $k$  is a constant factor that depends on material specifications. These two factors can change according to the fatigue criteria that are used. Considering the different MFC, in eqns 11, 12, 13, and 14 are presented the approaches used for computing  $k$  and  $S$  parameters. It is interesting to notice that all the  $k$  parameters are functions of  $\sigma_f$  and  $\tau_f$ . Indeed, its ratio is represented in the formulae through  $r_{\tau/\sigma}$  that is defined by eqn 15. With respect to the variable  $S$ , it is interesting to notice that the Papadopoulos criterion takes into account the max octahedral stress  $\sigma_{h,max}$ , while the others consider stresses that are connected to the critical plane, such as  $\sigma_{c,max}$  for the Findley criterion,  $\sigma_{c,a}$  for the Matake criterion, and  $\sigma_{c,max}/\tau_{c,a}$  in Susmel *et al.* criterion.

$$DP = \tau_{c,a} + kS \quad (10)$$

$$DP_{Findley} = \tau_{c,a} + \frac{2r_{\tau/\sigma} - 1}{2\left(\sqrt{r_{\tau/\sigma}} - r_{\tau/\sigma}^2\right)} \sigma_{c,max} \quad (11)$$

$$DP_{Matake} = \tau_{c,a} + (2r_{\tau/\sigma} - 1)\sigma_{c,a} \quad (12)$$

$$DP_{Susmel \text{ et al.}} = \tau_{c,a} + \left( \tau_f - \frac{\sigma_f}{2} \right) \frac{\sigma_{c,max}}{\tau_{c,a}} \quad (13)$$

$$DP_{Papadopoulos} = \tau_{c,a} + \left( \frac{3}{2}(2r_{\tau/\sigma} - 1) \right) \sigma_{h,max} \quad (14)$$

where

$$r_{\tau/\sigma} = \tau_f / \sigma_f \quad (15)$$

For the identification of the critical plane  $(\phi_c, \theta_c)$ , the Findley criterion asserts that the critical plane is the one in which the DP assumes its maximum value (eqn 16). On the contrary, the other MFC agree in defining the critical plane as the plane in which the tangential stress component  $\tau_{c,a}$  reaches its maximum value (eqn 18). For this reason, by applying the Findley criterion, it is possible to obtain critical planes with a different orientation than the critical planes obtained by implementing the other criteria.

$$(\phi_c, \theta_c) \rightarrow \max_{\phi, \theta} \{ \tau_{n,a}(\phi, \theta) + kS(\phi, \theta) \} \quad (16)$$

$$(\phi_c, \theta_c) \rightarrow \max_{\phi, \theta} \{ \tau_{n,a}(\phi, \theta) \} \quad (17)$$

### 3 MATERIAL AND METHOD

#### 3.1 Presentation of the general approach

In the presented work, two different analyses (RG and STBF) were performed through numerical techniques on the same gear geometry. For each simulation, considering ref. [11], the result was the same  $\sigma_{Flim}$ . Thanks to this numerical approach, it is possible to compute the stress tensor  $\bar{\sigma}_{(t)}$  in the critical region (tooth root). In other words, it is possible to extrapolate the stress history of the studied gear on each of the  $N$  nodes that belong to the tooth root fillet (in which failure may occur). Consequently, if a fatigue criterion is used for investigating the stress history, it is possible to:

1. Individuate the critical plane for each point  $(\theta_c, \phi_c(N))$ .
2. Evaluate the DP in each critical plane (eqn 10 applied on each node).
3. Identify the critical point in which the damage parameter assumes the maximum value

$$\left( \max_N \{ (\tau_{c,a} + kS) \} \right) .$$

This procedure can be used both for RG and STBF analyses. As mentioned in the previous paragraphs, the  $f_{korr}$  factor can be defined as the ratio between the maximum DP of the STBF condition and the RG one. This factor takes into consideration the different aspects that may cause rupture for tooth bending failure (eqn 18). The overall approach can be carried out by applying different MFCs. The FEA and how the previously mentioned criteria were implemented in this work are the future objects of the next sections.

$$f_{korr} = \frac{\max_N \{(\tau_{c,a} + kS)\}_{STBF}}{\max_N \{(\tau_{c,a} + kS)\}_{RG}} \quad (18)$$

The above-mentioned procedure can be repeated, varying the parameters  $\sigma_f$  and  $\tau_f$ . Indeed,  $\bar{\sigma}_f(t)$  obtained with FEA of gears set with typical isotropic steel properties, i.e. a Young modulus equal to 205 GPa and a Poisson's ratio of 0.3, can be processed with any value of  $\sigma_f$  and  $\tau_f$ . In this way, it is possible to investigate the relationship between  $f_{korr}$  and material-related parameters. More specifically, to explore plausible ranges of combinations of  $\sigma_f$  and  $\tau_f$ , it is more useful to consider  $\sigma_f$  and  $r_{\tau/\sigma}$ . More specifically, considering a wide spectrum of materials, as reported in ref. [48], it is possible to range from  $r_{\tau/\sigma} = 0.5$  (for NiCrMo steel, 75–80 tons) to  $r_{\tau/\sigma} = 0.95$  (for nodular cast iron). With respect to  $\sigma_f$ , it is possible to range from  $\sigma_f = 150$  MPa (for NiCr cast iron) to  $\sigma_f = 1500$  MPa (for VAR 9310). Moreover, the results of the implementation of the MFC of Susmel *et al.* are dependent on both  $\sigma_f$  and  $\tau_f$ ; the other MFCs are functions solely of  $r_{\tau/\sigma}$ .

### 3.2 Finite element analysis

In this research, the same gear geometry presented in ref. [33] has been simulated in both the STBF and RG conditions. The geometry was created through KISSsoft® having the parameters listed in Table 1. The geometrical model was imported in the open-source FE software Salome-Meca/Code\_Aster in which the two different tests (RG and STBF) were simulated.

Table 1: Geometrical parameter of the simulated gear according to ref. [33].

Description	Symbol	Unit	Value
Normal module	$m_n$	[mm]	4
Normal pressure angle	$\alpha_n$	[°]	20
Number of teeth	$z$	[-]	28
Face width	$b$	[mm]	30
Profile shift coefficient	$x$	[-]	0
Dedendum coefficient	$h_{fp}^*$	[-]	1.25
Root radius factor	$\rho_{fp}^*$	[-]	0.38
Addendum coefficient	$h_{ap}^*$	[-]	1

To reduce the computational effort of the simulations, some simplifications in the numerical model were made. In particular, considering the STBF test, only a quarter of each gear was modeled, and it is possible to use such simplification exploiting symmetries of the inspected gears. Moving to the RG analysis, due to the fact that the gears are meshing, it was possible to simulate only one half of the gears (the gear was modelled for half of the width). For each geometry, an extruded mesh was created, and particular attention was given to the teeth on which the contact occurs. In such regions, an improved mesh using hexahedrons was created (Fig. 3). Non-linear simulations have been carried out, setting 40 time-steps (along the period  $T$ ) for the loading cycle. It is important to notice that the nonlinearity of the simulation is due to the contact and not to the property of the material.

In Fig. 1a and 1b, it is possible to see the models that have been developed for the RG and STBF simulations. In the meshing model (RG), the two gears were fixed on their axis and positioned at an appropriate center distance. In addition, the rotation was imposed on the driving gear while a resistant torque was assigned to the driven one. In the pulsatory test (STBF), a cyclic force with  $R = 0.1$  was applied to the anvil, and as explained in the previous paragraph, the radial symmetry was used. According to the international standard ISO 6336-3 [11], the resistant torque applied in the RG simulation produced a stress  $\sigma_F$  that was equal to

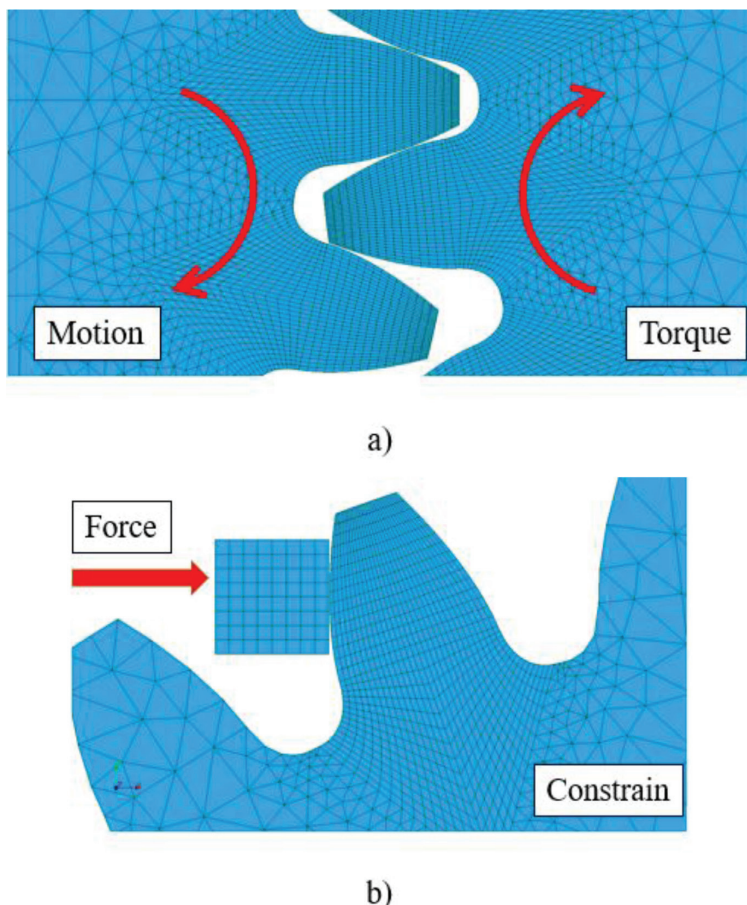


Figure 3: Finite element models of RG (a) and STBF (b) tests.

the one set in the pulsatory model. The same steel properties have been assigned to the two models thanks to a proper code. After simulations ran, the stress tensor  $\bar{\sigma}_{(t)}$  was extracted in the analysis region (tooth root fillet).

Numerical analysis were performed in the elastic field of the material, therefore, it was possible, just running two simulations (one STBF and one RG), to evaluate rapidly different materials with the same elastic module  $E$ . In fact, in this work, 2025 different combinations of  $\sigma_f$  and  $r_{\tau/\sigma}$  are reproduced, i.e. 45 values equally distributed between  $\sigma_f = 150$  MPa and  $\sigma_f = 1500$  MPa  $\times$  45 values equally distributed between  $r_{\tau/\sigma} = 0.5$  and  $r_{\tau/\sigma} = 0.95$ . The  $f_{korr}$  (according to the different MFC and different materials) have been calculated following the workflow presented in the previous section.

#### 4 RESULTS AND DISCUSSION

The main results are presented in Fig. 4. In the figure, the different values of  $f_{korr}$  computed for different MFC (in different colors) and for different material properties, i.e.  $\sigma_f$  and  $r_{\tau/\sigma}$  (and consequently  $\tau_f$ ), are reported according to ref. [48]. In addition, some typical materials for gear manufacturing are reported in the figure, i.e.

- 18NiCrMo5 ( $r_{\tau/\sigma} = 0.51$ ,  $\sigma_f = 660$ );
- 31CrMo12 ( $r_{\tau/\sigma} = 0.58$ ,  $\sigma_f = 628$ );
- 42CrMoS4 ( $r_{\tau/\sigma} = 0.64$ ,  $\sigma_f = 526$ );
- 39NiCrMo3 ( $r_{\tau/\sigma} = 0.72$ ,  $\sigma_f = 367$ );
- C34N ( $r_{\tau/\sigma} = 0.79$ ,  $\sigma_f = 190$ );
- Inoculated cast iron ( $r_{\tau/\sigma} = 0.88$ ,  $\sigma_f = 178$ ).

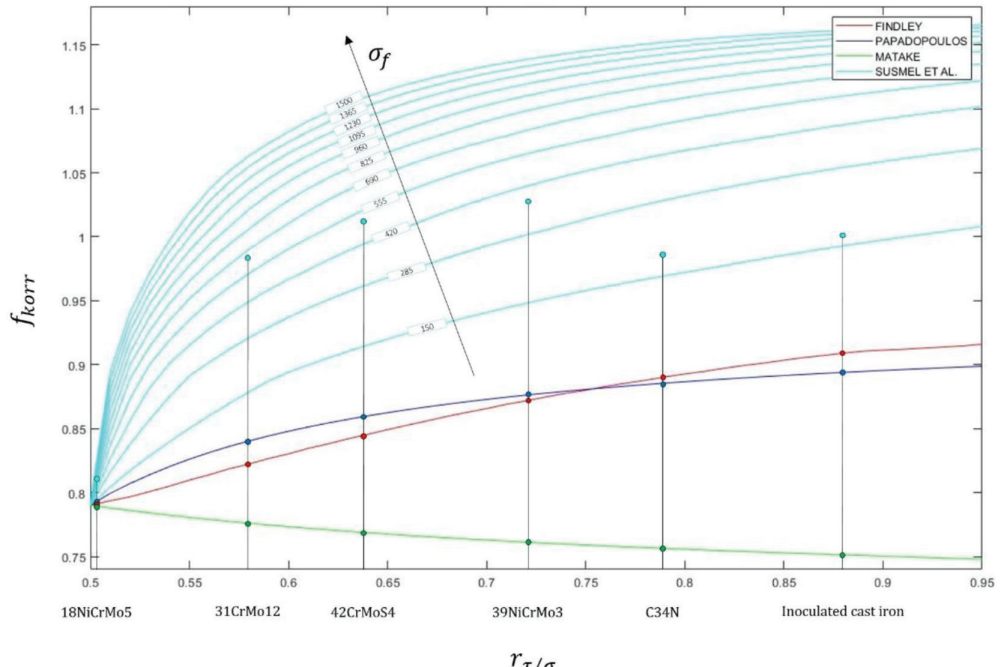


Figure 4: Effect of material properties on  $f_{korr}$  for different multiaxial fatigue criteria.

It is interesting to notice that all the criteria agree for the value of  $r_{\tau/\sigma} = 0.5$  to  $f_{korr} = 0.79$ . This can be explained by the fact that all MFC agree to zeroing the  $k$  value (eqn 10) when  $r_{\tau/\sigma} = 0.5$ . Therefore, for  $r_{\tau/\sigma} = 0.5$ , the DP is due solely to  $\tau_{c,a}$  for all the MFC.

It is possible to notice that the Susmel *et al.* criterion (in cyan) proposes multiple solutions of  $f_{korr}$  for the same  $r_{\tau/\sigma}$ . More specifically, at the same  $r_{\tau/\sigma}$ , the value of  $f_{korr}$  increases as  $\sigma_f$  increases, and this effect is less marked for high  $r_{\tau/\sigma}$  values. The other MFCs, as expected, turn out to be functions of  $r_{\tau/\sigma}$  only. The values of  $f_{korr}$  calculated implementing the Susmel *et al.* criterion are always higher than the values proposed by the other criteria. Moreover, the MFC of Susmel *et al.* tend to exceed  $f_{korr} = 1$  for relatively high  $r_{\tau/\sigma}$  (and/or  $\sigma_f$ ) values. This means that, in agreement with this MFC, for some  $r_{\tau/\sigma}$  conditions, the  $\bar{\sigma}_{(t)}$  induced in the STBF loading condition could be more severe than that of  $\bar{\sigma}_{(t)}$  induced in the RG loading condition. On the contrary, the other MFCs always propose  $f_{korr} < 0.95$ .

It can be easily observed how the results of  $f_{korr}$  obtained with the implementation of Findley (red in Fig. 4) and Papadopoulos (in blue) criteria are very similar in trend (monotone increasing with  $r_{\tau/\sigma}$ ) and in values. More specifically, it can be observed that for the value of  $r_{\tau/\sigma} = 0.76$ , the two criteria lead to the same value of  $f_{korr} = 0.88$ . For  $r_{\tau/\sigma} = 0.76$ , Findley's criterion leads to slightly higher  $f_{korr}$  results, while the opposite occurs for  $r_{\tau/\sigma} = 0.76$  values.

The Matake criterion (green in Fig. 4) shows a monotonically decreasing trend of  $f_{korr}$  with respect to  $r_{\tau/\sigma}$ . This is the only criterion that shows such a trend. In addition, this criterion shows the least variability (with respect to the other criteria) of  $f_{korr}$  as  $r_{\tau/\sigma}$  varies. Therefore, Matake's criterion results are the most cautionary of the MFC, ranging from a  $f_{korr} = 0.75$  to  $f_{korr} = 0.79$ .

## 5 CONCLUSIONS

In this work, a method for calculating the coefficient  $f_{korr}$ , according to different MFC (i.e. Findley, Matake, Papadopoulos, and Susmel *et al.*), is presented. This coefficient permits to exploit results obtained from the STBF tests for the gear design phase. In the proposed method, results of FEA were analyzed exploiting different critical plane-based MFC. Data required for applying this approach are  $\tau_f$  and  $\sigma_f$ , which depend on material properties that have been varied systematically to simulate a wide range of possible materials for gear manufacturing, i.e.  $\sigma_f = 150 - 1500$  MPa (each 30 MPa) and  $r_{\tau/\sigma} = \tau_f/\sigma_f = 0.5 - 0.95$  (each 0.01). This approach was applied to a specific gear geometry exploited in previous studies by the authors' research group. The results, in terms of the effect of  $\tau_f$  and  $\sigma_f$  on  $f_{korr}$  as the MFC varies, show the following relationships:

- All MFC agree that when  $r_{\tau/\sigma} = 0.5$  then  $f_{korr} = 0.79$ ;
- All MFC show a monotonic crescent relationship of  $f_{korr}$  with  $\tau_f/\sigma_f$  except for the Matake criterion, which, in turn, has the least variability of  $f_{korr}$ . The values it assumes are always below 0.79, and, therefore, it reveals to be the most conservative criterion;
- The criterion of Susmel *et al.* is the only one that is not a function of  $r_{\tau/\sigma}$  only and leads to values of  $f_{korr}$  higher than all other criteria (also above the unity). Therefore, this classifies it as the least conservative criterion;
- The criteria of Findley and Papadopoulos lead to very similar values of  $f_{korr}$ , which are around those also observed experimentally.

However, these results were obtained by simulating a single gear geometry. Future studies should aim to study the effect of geometry on these outcomes. Moreover, another aspect

worth to investigating is the non-continuity points of the  $f_{korr}(\sigma_f, r_{\tau/\sigma})$  functions. Future studies would investigate whether the critical node for RG and STBF testing is the same or whether the shift of the critical point toward the tooth flank (or tooth root) can be identified as a function of material properties and/or type of test.

## REFERENCES

- [1] Vullo, V., *Gears*. Springer International Publishing, 2020.
- [2] Concli, F., Cortese, L., Vidoni, R., Nalli, F. & Carabin, G., A mixed FEM and lumped-parameter dynamic model for evaluating the modal properties of planetary gearboxes. *Journal of Mechanical Science and Technology*, **32**(7), pp. 3047–3056, 2018. <https://doi.org/10.1007/s12206-018-0607-9>
- [3] Blake, J.W. & Cheng, H.S., A surface pitting life model for spur gears: Part I—Life prediction. *J. Tribol.*, **113**, pp. 712–718, 1991. <https://doi.org/10.1115/1.2920683>
- [4] Wu, S. & Cheng, H.S., Sliding wear calculation in spur gears. *J. Tribol.*, **115**, pp. 493–500, 1993. <https://doi.org/10.1115/1.2921665>
- [5] Li, S. & Kahraman, A., A scuffing model for spur gear contacts. *Mechanism and Machine Theory*, **156**, p. 104161, 2021. <https://doi.org/10.1016/j.mechmachtheory.2020.104161>
- [6] Liu, H., Liu, H., Zhu, C. & Zhou, Y., A review on micropitting studies of steel gears. *Coatings*, **9**(1), p. 42, 2019. <https://doi.org/10.3390/coatings9010042>
- [7] Fernandes, P.J.L., Tooth bending fatigue failures in gears. *Engineering Failure Analysis*, **3**(3), pp. 219–225, 1996. [https://doi.org/10.1016/1350-6307\(96\)00008-8](https://doi.org/10.1016/1350-6307(96)00008-8)
- [8] Hong, I.J., Kahraman, A. & Anderson, N., A rotating gear test methodology for evaluation of high-cycle tooth bending fatigue lives under fully reversed and fully released loading conditions. *International Journal of Fatigue*, **133**, p. 105432, 2020. <https://doi.org/10.1016/j.ijfatigue.2019.105432>
- [9] Pantazopoulos, G.A., Bending fatigue failure of a helical pinion bevel gear. *Journal of Failure Analysis and Prevention*, **15**(2), pp. 219–226, 2015. <https://doi.org/10.1007/s11668-015-9947-2>
- [10] Bretl, N., Schurer, S., Tobie, T., Stahl, K. & Höhn, B.R., Investigations on tooth root bending strength of case hardened gears in the range of high cycle fatigue. In *American Gear Manufacturers Association Fall Technical Meeting*, pp. 103–118, 2013.
- [11] ISO 6336-3:2006, *Calculation of Load Capacity of Spur and Helical Gears, Part 3: Calculation of Tooth Bending Strength*. Standard, Geneva, CH, 2006.
- [12] ANSI/AGMA 2001-D04, *Fundamental Rating Factors and Calculation Methods for Involute Spur and Helical Gear Teeth*. American Gear Manufacturers Association, Alexandria, 2004.
- [13] Rao, S.B. & McPherson, D.R., Experimental characterization of bending fatigue strength in gear teeth. *Gear Technology*, **20**(1), pp. 25–32, 2003.
- [14] Benedetti, M., Fontanari, V., Höhn, B.R., Oster, P. & Tobie, T., Influence of shot peening on bending tooth fatigue limit of case hardened gears. *International Journal of Fatigue*, **24**(11), pp. 1127–1136, 2002. [https://doi.org/10.1016/S0142-1123\(02\)00034-8](https://doi.org/10.1016/S0142-1123(02)00034-8)
- [15] McPherson, D.R. & Rao, S.B., Methodology for translating single-tooth bending fatigue data to be comparable to running gear data. *Gear Technology*, 42–51, 2008.
- [16] Dobler, D.I.A., Hergesell, I.M. & Stahl, I.K., Increased tooth bending strength and pitting load capacity of fine-module gears. *Gear Technology*, **33**(7), pp. 48–53, 2016.
- [17] Concli, F., Tooth root bending strength of gears: dimensional effect for small gears having a module below 5 mm. *Applied Science*, **11**, p. 2416, 2021. <https://doi.org/10.3390/app11052416>

- [18] Gorla, C., Conrado, E., Rosa, F. & Concli, F., Contact and bending fatigue behaviour of austempered ductile iron gears. *Proceedings of the Institution of Mechanical Engineers, Part C: Journal of Mechanical Engineering Science*, **232**(6), pp. 998–1008, 2018. <https://doi.org/10.1177/0954406217695846>
- [19] McPherson, D.R. & Rao, S.B., *Mechanical Testing of Gears*. Materials Park, OH: ASM International, 2000, pp. 861–872.
- [20] Concli, F., Fraccaroli, L. & Maccioni, L., Gear root bending strength: A new multiaxial approach to translate the results of single tooth bending fatigue tests to meshing gears. *Metals*, **11**(6), p. 863, 2021. <https://doi.org/10.3390/met11060863>
- [21] Concli, F., Maccioni, L., Fraccaroli, L. & Cappellini, C., Effect of gear design parameters on stress histories induced by different tooth bending fatigue tests: a numerical-statistical investigation. *Applied Sciences*, **12**(8), p. 3950, 2022. <https://doi.org/10.3390/app12083950>
- [22] Rettig, H., Ermittlung von Zahnfußfestigkeitskennwerten auf Verspannungsprüfständen und Pulsatoren-Vergleich der Prüfverfahren und der gewonnenen Kennwerte. *Antriebstechnik*, **26**, pp. 51–55, 1987.
- [23] Stahl, K., Lebensdauer Statistik: Abschlussbericht, Forschungsvorhaben nr. 304. *Tech. Rep.* 580, 1999.
- [24] Concli, F., Austempered Ductile Iron (ADI) for gears: Contact and bending fatigue behavior. *Procedia Structural Integrity*, **8**, pp. 14–23, 2018. <https://doi.org/10.1016/j.prostr.2017.12.003>
- [25] Bonaiti, L., Concli, F., Gorla, C. & Rosa, F., Bending fatigue behaviour of 17-4 PH gears produced via selective laser melting. *Procedia Structural Integrity*, **24**, pp. 764–774, 2019. <https://doi.org/10.1016/j.prostr.2020.02.068>
- [26] Gasparini, G., Mariani, U., Gorla, C., Filippini, M. & Rosa, F., Bending 367 Fatigue Tests of Helicopter Case Carburized Gears: Influence of Material, Design 368 and Manufacturing Parameters. In AGMA (Ed.), *American Gear Manufacturers Association 369 (AGMA) Fall Technical Meeting*, 2008, pp. 131–142.
- [27] Gorla, C., Rosa, F., Concli, F. & Albertini, H., Bending fatigue strength of innovative gear materials for wind turbines gearboxes: Effect of surface coatings. In ASME *International Mechanical Engineering Congress and Exposition*. American Society of Mechanical Engineers, 2012, Vol. 45233, pp. 3141–3147. <https://doi.org/10.1115/IMECE2012-86513>
- [28] Gorla, C., Rosa, F., Conrado, E. & Concli, F., Bending fatigue strength of case carburized and nitrided gear steels for aeronautical applications. *International Journal of Applied Engineering Research*, **12**(21), pp. 11306–11322, 2017.
- [29] Rao, S.B., Schwanger, V., McPherson, D.R. & Rudd, C., Measurement and validation of dynamic bending stresses in spur gear teeth. In *International Design Engineering Technical Conferences and Computers and Information in Engineering Conference*, 2005, Vol. 4742, pp. 755–764. <https://doi.org/10.1115/DETC2005-84419>
- [30] Wagner, M., Isaacson, A., Knox, K. & Hylton, T., Single tooth bending fatigue testing at any r ratio. In *2020 AGMA/ABMA Annual Meeting*. AGMA American Gear Manufacturers Association, 2020.
- [31] Bonaiti, L., Bayoumi, A.B.M., Concli, F., Rosa, F. & Gorla, C., Gear root bending strength: a comparison between Single Tooth Bending Fatigue Tests and meshing gears. *Journal of Mechanical Design*, pp. 1–17, 2021. <https://doi.org/10.1115/1.4050560>
- [32] Hong, I., Teaford, Z. & Kahraman, A., A comparison of gear tooth bending fatigue lives from single tooth bending and rotating gear tests. *Forschung im Ingenieurwesen*, pp. 1–13, 2021. <https://doi.org/10.1007/s10010-021-00510-w>

- [33] Conrado, E., Gorla, C., Davoli, P. & Boniardi, M., A comparison of bending fatigue strength of carburized and nitrided gears for industrial applications. *Engineering Failure Analysis*, **78**, pp. 41–54, 2017. <https://doi.org/10.1016/j.engfailanal.2017.03.006>
- [34] Savaria, V., Bridier, F. & Bocher, P., Predicting the effects of material properties gradient and residual stresses on the bending fatigue strength of induction hardened aeronautical gears. *International Journal of Fatigue*, **85**, pp. 70–84, 2016. <https://doi.org/10.1016/j.ijfatigue.2015.12.004>
- [35] Crossland, B., Effect of large hydrostatic pressures on the torsional fatigue strength of an alloy steel. In *Proc. Int. Conf. on Fatigue of Metals*. Institution of Mechanical Engineers London, 1956, Vol. 138, pp. 12–12.
- [36] Hotait, M.A. & Kahraman, A., Estimation of bending fatigue life of hypoid gears using a multiaxial fatigue criterion. *Journal of Mechanical Design*, **135**(10), p. 101005, 2013. <https://doi.org/10.1115/1.4025024>
- [37] Liu, Y. & Mahadevan, S., A unified multiaxial fatigue damage model for isotropic and anisotropic materials. *International Journal of Fatigue*, **29**(2), pp. 347–359, 2007. <https://doi.org/10.1016/j.ijfatigue.2006.03.011>
- [38] Findley, W.N., A theory for the effect of mean stress on fatigue of metals under combined torsion and axial load or bending. *Journal of Engineering for Industry*, **81**(4), pp. 301–305. <https://doi.org/10.1115/1.4008327>
- [39] Concli, F., Maccioni, L. & Bonaiti, L., Reliable gear design: Translation of the results of single tooth bending fatigue tests through the combination of numerical simulations and fatigue criteria. *WIT Transactions on Engineering Sciences*, **130**, pp. 111–122, 2021. <https://doi.org/10.2495/cmem210101>
- [40] Matake, T., An explanation on fatigue limit under combined stress. *Bulletin of JSME*, **20**(141), pp. 257–263, 1977. <https://doi.org/10.1299/jsme1958.20.257>
- [41] McDiarmid, D.L., Fatigue under out-of-phase biaxial stresses of different frequencies. In *Multiaxial Fatigue*. ASTM International, 1985. <https://doi.org/10.1520/STP36245S>
- [42] Papadopoulos, I.V., A high cycle fatigue criterion applied in biaxial and triaxial out-of-phase stress conditions. *Fatigue & Fracture of Engineering Materials & Structures*, **18**(1), pp. 79–91, 1995. <https://doi.org/10.1111/j.1460-2695.1995.tb00143.x>
- [43] Susmel, L., Tovo, R. & Lazzarin, P., The mean stress effect on the high-cycle fatigue strength from a multiaxial fatigue point of view. *International Journal of Fatigue*, **27**(8), pp. 928–943, 2005. <https://doi.org/10.1016/j.ijfatigue.2004.11.012>
- [44] Concli, F., Maccioni, L., Fraccaroli, L. & Bonaiti, L., Early crack propagation in single tooth bending fatigue: Combination of finite element analysis and critical-planes fatigue criteria. *Metals*, **11**(11), p. 1871, 2021. <https://doi.org/10.3390/met11111871>
- [45] Karolczuk, A. & Papuga, J., Recent progress in the application of multiaxial fatigue criteria to lifetime calculations. *Procedia Structural Integrity*, **23**, pp. 69–76, 2019. <https://doi.org/10.1016/J.PROSTR.2020.01.065>
- [46] Concli, F. & Maccioni, L., Critical planes criteria applied to gear teeth: Which one is the most appropriate to characterize crack propagation. *WIT Trans. Eng. Sci.*, **133**, pp. 15–25, 2021. <https://doi.org/10.2495/MC210021>
- [47] Papadopoulos, I.V., Critical plane approaches in high-cycle fatigue: on the definition of the amplitude and mean value of the shear stress acting on the critical plane. *Fatigue & Fracture of Engineering Materials & Structures*, **21**(3), pp. 269–285, 1998. <https://doi.org/10.1046/j.1460-2695.1998.00459.x>
- [48] Susmel, L., On the overall accuracy of the Modified Wöhler Curve Method in estimating high-cycle multiaxial fatigue strength. *Frattura ed Integrità Strutturale*, **5**(16), pp. 5–17, 2011. <https://doi.org/10.3221/IGF-ESIS.16.01>